



HAL
open science

Electronic Structure and Geometry of the Lowest 2LMCT State of Fe(III) Potential Fluorescent Emitters

Tabea Huss, Isabelle M Dixon

► **To cite this version:**

Tabea Huss, Isabelle M Dixon. Electronic Structure and Geometry of the Lowest 2LMCT State of Fe(III) Potential Fluorescent Emitters. *Inorganic Chemistry*, 2023, 62 (10), pp.4284-4290. 10.1021/acs.inorgchem.2c04407 . hal-04028149

HAL Id: hal-04028149

<https://hal.science/hal-04028149>

Submitted on 14 Mar 2023

HAL is a multi-disciplinary open access archive for the deposit and dissemination of scientific research documents, whether they are published or not. The documents may come from teaching and research institutions in France or abroad, or from public or private research centers.

L'archive ouverte pluridisciplinaire **HAL**, est destinée au dépôt et à la diffusion de documents scientifiques de niveau recherche, publiés ou non, émanant des établissements d'enseignement et de recherche français ou étrangers, des laboratoires publics ou privés.

Copyright

Electronic structure and geometry of the lowest $^2\text{LMCT}$ state of Fe(III) potential fluorescent emitters

*Tabea Huss† and Isabelle M. Dixon**

Laboratoire de Chimie et Physique Quantiques

Universite de Toulouse, CNRS, Universite Toulouse III - Paul Sabatier

F-31062 Toulouse, France

* isabelle.dixon@irsamc.ups-tlse.fr

† Fritz-Haber-Institut der Max-Planck-Gesellschaft, Faradayweg 4-6, 14195 Berlin, Germany.

ABSTRACT.

Metal complexes with a $3d^5$ electron count are emerging as an alternative to $4d^6$ -based photosensitizers, emitters, or photoredox catalysts. In recent years several Fe(II) potential emitters have been proposed, based on strongly donating ligand sets. Those tend to facilitate oxidation to their $3d^5$ species, whose photophysics is based on low-lying ligand-to-metal charge transfer (LMCT) states. The geometry and electronic structure of $^3\text{LMCT}$ states are unveiled in this work.

Introduction

The use of earth abundant metal complexes with light-triggered applications is highly desirable for environmental, sustainability, and economic issues, to the least. This general consensus has stimulated intense research efforts and is an actively pursued goal in photophysics,^{1,2,3,4} photobiology,⁵ or photoredox catalysis.⁶ Focusing on iron, the most abundant transition metal in the Earth's crust,⁷ the past few years have witnessed spectacular extensions in charge transfer excited state lifetimes of iron complexes, which have jumped from sub-ps⁸ to ps^{9,10,11} to ns timescales,^{12,13,14} through the use of strongly donating ligands. These ligands, which destabilize otherwise low-lying metal centred states but might favor the Fe(III) oxidation state, display N-heterocyclic or mesoionic carbene donor sites, amido ligands, and/or cyclometallating ligands, combined with π -accepting polypyridine-type moieties. Exploring the photophysical capabilities of Fe(II) cyclometallated complexes with DFT methods,¹⁵ we could foresee their potential as panchromatic absorbers¹⁶ and infrared emitters¹⁷ following $^3\text{MLCT}$ - ^3MC state inversion using this class of ligands, a fact that has been experimentally confirmed recently.¹⁸ In the same years their potential as dyes for dye-sensitized solar cells was also reported, in which they would advantageously stand in for ruthenium.¹⁹ In case facile or even spontaneous Fe(II) \rightarrow Fe(III) oxidation should be avoided, the use of electron-withdrawing substituents could moderate this tendency^{17,19,20} and stabilize the Fe(II) form, but in the absence of electroattracting groups, both Fe(II) complexes^{21,22,23} and Fe(III) complexes^{24,25,26} have been isolated.

The motivation for this work is to characterize the potentially emitting state of Fe(III) complexes, as no theoretical data is currently available on their optimized $^3\text{LMCT}$ states, to the best of our knowledge. The same series of six complexes is reported in this work, as previously studied in the Fe(II) oxidation state: Fe(tpy)(N[^]C[^]N)²⁺, Fe(tpy)(N[^]N[^]C)²⁺, Fe(N[^]C[^]N)²⁺,

$\text{Fe}(\text{N}^{\wedge}\text{N}^{\wedge}\text{C})_2^+$ and $\text{Fe}(\text{N}^{\wedge}\text{N}^{\wedge}\text{C})(\text{N}^{\wedge}\text{C}^{\wedge}\text{N})^+$, as well as $\text{Fe}(\text{tpy})_2^{3+}$ as the non-cyclometallated reference (Figure 1) (tpy = 2,2':6',2''-terpyridine ; $\text{N}^{\wedge}\text{N}^{\wedge}\text{C}$ = 6-phenyl-2,2'-bipyridine, $\text{N}^{\wedge}\text{C}^{\wedge}\text{N}$ = 2,6-dipyridylbenzene, the latter two binding the metal in a tridentate fashion following deprotonation of the phenyl ring). The manuscript is organized as follows: the DFT-optimized ground state electronic structure is first presented, followed by a TD-DFT calculation at the ground state geometry to identify the excited states of interest. Then the lowest $^3\text{LMCT}$ state is optimized by TD-DFT, and discussed in terms of electronic structure and geometry. The reaction coordinate connecting the ground state and the $^3\text{LMCT}$ state is unveiled for the first time, which could be helpful in the future design of efficient iron-based emitters or photoredox catalysts.

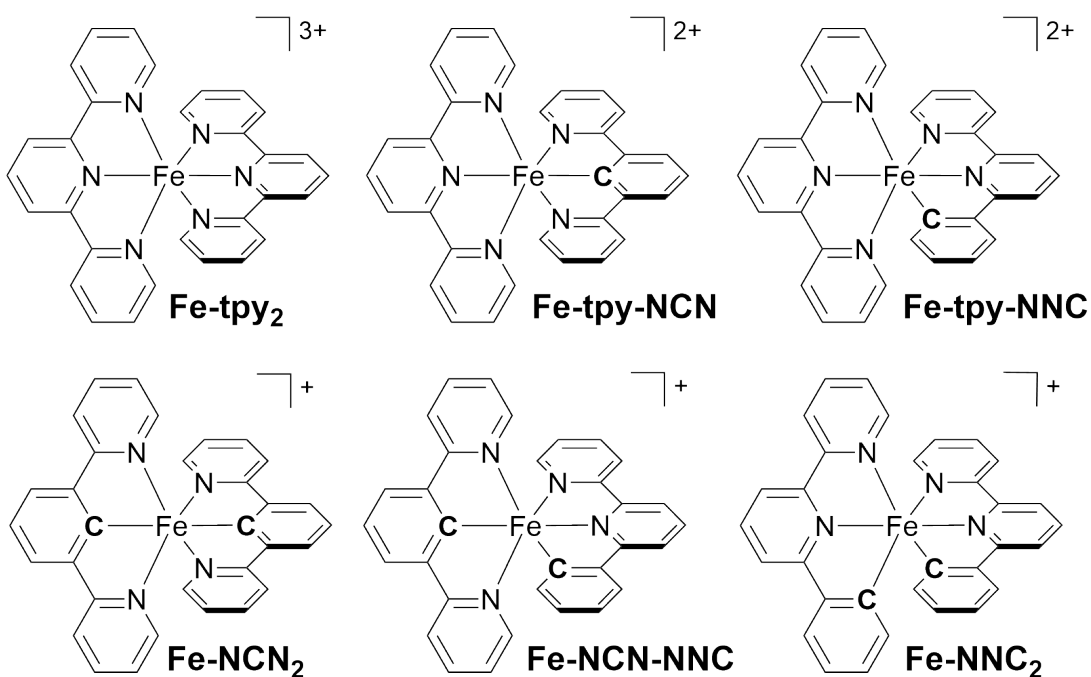


Figure 1 : Chemical structures and abbreviations for the studied complexes.

Computational details

Ground state geometries were optimized with doublet spin multiplicity within the unrestricted Kohn-Sham formalism with the B3LYP* functional,^{27,28} with D3BJ dispersion,^{29,30} using ZORA³¹

and its associated basis set ZORA-def2-TZVP(-f) to account for scalar relativistic effects. TD-DFT calculations were performed following the Tamm-Dancoff approximation and used the same basis set. TD-DFT excited state optimizations were performed using 10 roots (12 roots for the least symmetric **Fe-NNC-NCN** complex). All calculations were performed in a standard solvent for photophysical studies of metal complexes, acetonitrile (CPCM), with Orca5³² using the RIJCOSX approximation and the def2/j auxiliary basis set.³³ TD-DFT calculations were repeated (at the CPCM(MeCN) geometries) in CH₂Cl₂, another common solvent for photophysics, to showcase the minor effect of a less polar medium on the electronic transitions of interest (Table S8). The molecular orbitals are plotted with Gabedit³⁴ using a contour isovalue of 0.04.

Ground state electronic structure

In their doublet ground state, Fe(III) d⁵ complexes possess a metal-based β -LUMO, a specificity that adds low-lying ligand-to-metal charge transfer (LMCT, π to d_{π}) transitions to the classical metal-to-ligand charge transfer (MLCT, d_{π} to π^*) and metal centered (MC, d_{π} to $d\sigma^*$) transitions commonly found in their Fe(II) d⁶ counterparts bearing π -accepting polypyridine ligands and σ - and π -donating cyclometallating ligands (Figure 2).¹⁶ The ligand set then defines the relative position of the occupied π and vacant π^* orbitals involved in these transitions with respect to the metallic d_{π} and $d\sigma^*$ orbitals, and their degree of mixing.^{35,36} Besides, there are two very-low-lying states, below noted GS' and GS'', corresponding to the other two distributions of two electrons in three β - d_{π} spin orbitals. GS, GS' and GS'' can be seen as the three sublevels of the doublet ground state, and are generally found within half an eV at the Franck-Condon geometries. As an example, GS' and GS'' have been optimized by TDDFT for two complexes in the series, **Fe-tpy-NNC** and **Fe-NNC₂**. GS' ended up 0.262 eV above ²GS for **Fe-tpy-NNC** and

0.352 eV above ^2GS for **Fe-NNC₂**. GS'' ended up 0.399 eV above ^2GS for **Fe-tpy-NNC** and 0.370 eV above ^2GS for **Fe-NNC₂** (electronic energy gaps). For a given complex, the geometries of ^2GS , GS' and GS'' are very similar (RMSD~0.06-0.07), as expected for a change in the occupation of nonbonding orbitals. The geometries of these TD-DFT optimized GS' and GS'' structures are provided as Supporting Information.

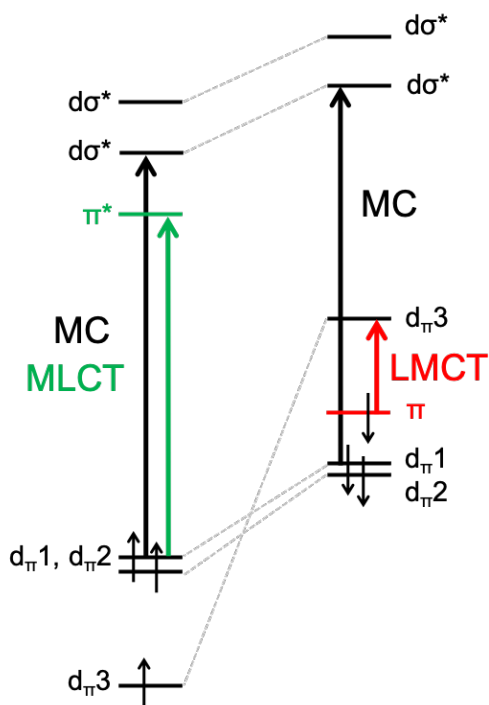


Figure 2: Single excitations of interest shown on the schematic MO diagram of the doublet ground state of Fe³⁺ d⁵ complexes (d_{π1} → d_{π3} and d_{π2} → d_{π3} excitations in the β spinorbital subset not shown).

The ground state MO diagram for Fe(tpy)₂³⁺ is shown in Figure 3. The others are provided as Supporting Information in Figures S1-S5.

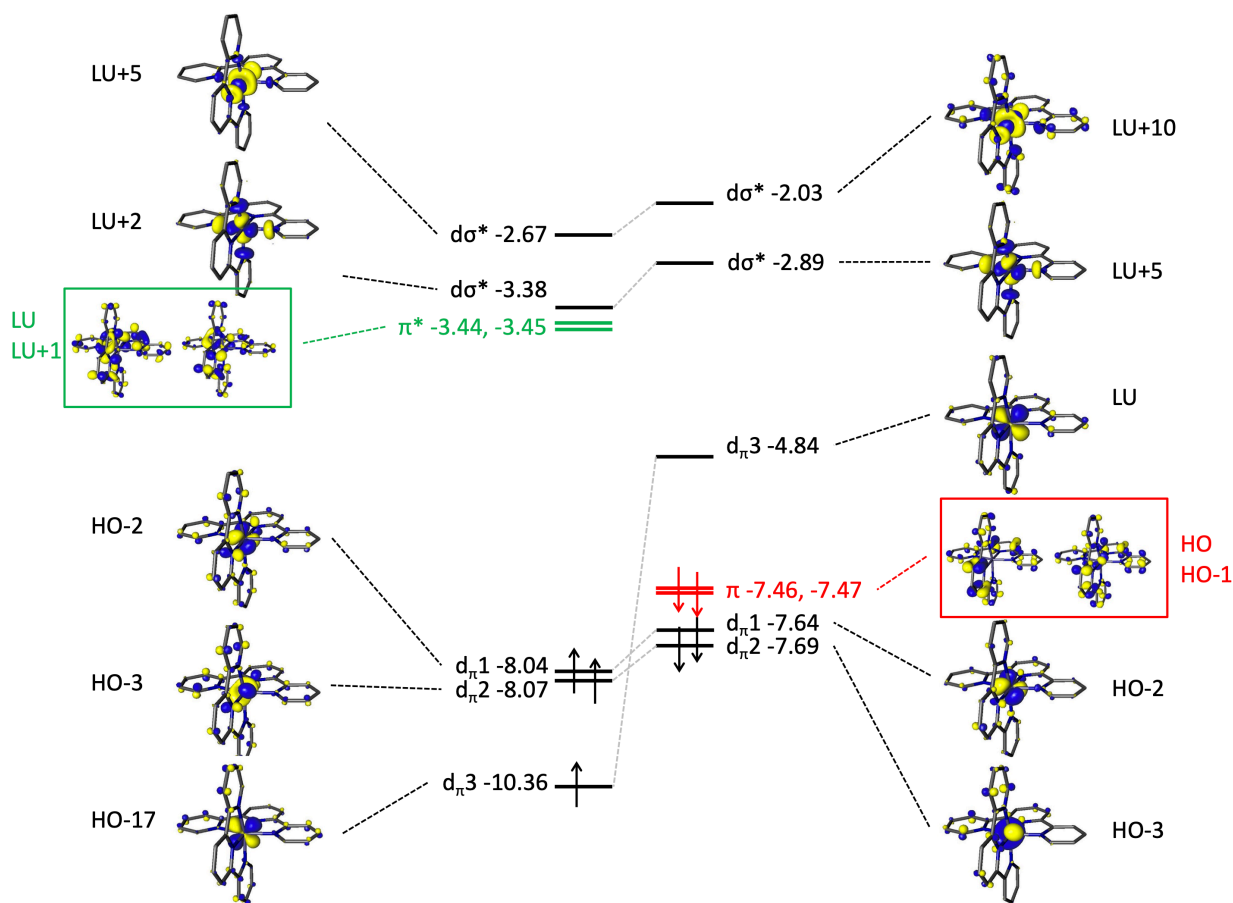


Figure 3: Selected MO diagram for the doublet ground state of $\text{Fe}(\text{tpy})_2^{3+}$ (eigenvalues in eV). In green the accepting orbital(s) to be populated for an excited MLCT state. In red, the donating orbital(s) to be depopulated for an excited LMCT state. Orbitals α -HO/ α -HO-1 (corresponding and very similar to β -HO/ β -HO-1) and β -LU+1/ β -LU+2 (corresponding and very similar to α -LU/ α -LU+1) not shown. Computed at the B3LYP* - D3BJ - ZORA-def2-TZVP(-f) level of theory in implicit MeCN (CPCM).

In the case of $\text{Fe}(\text{tpy})_2^{3+}$, herein abbreviated **Fe-tpy₂**, the ligand-based occupied π orbitals from which an electron is promoted to populate a $^3\text{LMCT}$ state are β -HOMO or β -HOMO-1. The presence of the metallic $d\sigma^*$ orbital as α -LUMO+2, almost degenerate with α -

LUMO/LUMO+1, enables us to foresee low-lying MC states originating from excitations in the α set of spin orbitals.

When tpy is replaced by N[^]N[^]C, i.e. for the dicationic complex **Fe-tpy-NNC** (Figure S1), the spacing between the lowest metallic $d\sigma^*$ orbital (α -LUMO+4) and the ligand-based π^* α -LUMO, now about 1 eV, should render MLCT states more competitive with MC states than without any cyclometallating ligand. Strong mixing between metal d_π and ligand π orbitals is found in orbitals β -HOMO-1 and β -HOMO-2. Both orbitals are then expected to be involved *both* in LMCT transitions (through their ligand-based component) and in the GS/GS'/GS'' transitions (through their metal-based component), via promotion of one electron into the metallic β -LUMO. The bis(cyclometallated) $\text{Fe}(\text{N}^{\wedge}\text{N}^{\wedge}\text{C})_2^+$ complex, abbreviated **Fe-NNC**, is different in two ways : (i) the LMCT-relevant ligand-based occupied π orbital is now β -HOMO-2, a π orbital localized on the phenyl rings of both ligands; (ii) the lowest metallic α - $d\sigma^*$ orbital is located almost 2 eV above the π^* α -LUMO, therefore MC states should be the least accessible in this case (Figure S2).

In the singly cyclometallated complex containing dipyritylbenzene, **Fe-tpy-NCN**, is observed the highest degree of mixing between metallic and ligand-based orbitals, in both α and β subsets, for symmetry reasons (Figure S3). The spacing between the lowest metallic $d\sigma^*$ orbital (α -LUMO+3) and the ligand-based π^* LUMO, is here reduced to 0.7 eV, therefore MC states are expected to be accessible. Its bis(cyclometallated) analogue, **Fe-NCN**, displays mixed metal/ligand orbitals in the α subset, and a lowest metallic $d\sigma^*$ orbital (α -LUMO+4) only 0.5 eV above the π^* α -LUMO (Figure S4). More noteworthy is the fact that the β -HOMO-2, from

which electron density will be taken in an LMCT-type excitation, is here composed of the antibonding combination of the two Fe-C sigma bonds.

Finally, in the monocationic **Fe-NNC-NCN**, the N[^]N[^]C ligand restores a significant spacing of 1.5 eV between the lowest metallic α -d σ^* orbital (LU+7) and the ligand-based α -LUMO (Figure S5). The highest ligand-based occupied π orbital is β -HOMO-2, a π orbital localized on the phenyl rings of both ligands, with a much larger contribution from the phenyl ring of the N[^]N[^]C ligand.

As a very brief summary of the previous Fe(II) study, the N[^]C[^]N ligand was shown to be a poor substitute for tpy, while the N[^]N[^]C ligand was foreseen to be beneficial, in terms of photophysical properties (destabilized MC states being correlated with extended MLCT lifetimes), as confirmed by experimental data.^{21,18} The same conclusions seem to be transposed to the Fe(III) oxidation state, based upon the ground state molecular orbital diagrams, with low-lying MC states in the case of **Fe-tpy**., **Fe-tpy-NCN**, **Fe-NCN**, and to a lesser extent **Fe-tpy-NNC**.

TD-DFT at the ground state geometry

In their doublet ground state geometries, all six complexes are characterized by planar tridentate ligands lying orthogonal to one another. The main features are extended Fe-N bonds when located trans to a formally anionic carbon atom (Table S1).

Tables S2-S7 gather the analysis of the TD-DFT results for the lowest excited states of all six complexes, computed at their respective relaxed ground state geometry. The reference state being a doublet spin state, both doublet and quartet states can be accessed upon single excitation, depending on the localization of donating and receiving orbitals. In the unrestricted Kohn-Sham

formalism, unphysical states with mixed doublet and quartet characters appear spin contaminated and should be discarded.

Consistent with the MC-stabilizing effect of one or two cyclometallating N[^]C[^]N ligands but MC-destabilizing effect of two N[^]N[^]C ligands we had observed in their Fe(II) congeners,¹⁶ the lowest excited states are of ⁴MC nature in all cases but **Fe-NNC₂**, which bears several charge transfer states below the MC states. From a photophysical perspective, the least favorable situations are found when the MC state is well below charge transfer states (i.e. with one or two N[^]C[^]N ligands). In the intermediate case, the MC states are quasi-degenerate with charge transfer states (i.e. **Fe-tpy**, and **Fe-tpy-NNC**).

It is noteworthy that charge transfer states of ligand-to-metal (LMCT), metal-to-ligand (MLCT) but also σ -bond to metal (SBMCT) and π -bond to metal (PBMCT) are found. Even if significantly higher oscillator strengths are expected for ¹MLCT excitations in Fe(II) complexes than for ³LMCT excitations in their Fe(III) counterparts,³⁷ exploitable oscillator strengths are predicted in this Fe(III) series (Tables S2-S7).

³LMCT state optimization

Excited state optimization of the lowest ³LMCT states was performed by TD-DFT. The intrinsically mixed character of the key orbitals involved in these organometallic complexes complicates the process and sometimes misleads the overlap-based excited state tracking procedures. Switching excited state tracking on or off at various stages of the calculations has eventually allowed us to achieve standard geometry optimization convergence in all cases but **Fe-tpy-NCN**, which converged to a looser level. The main structural parameters of the optimized ³LMCT states are given in Table S9. No obvious reaction coordinate for ³GS-to-

3 LMCT relaxation appears from the comparative analysis of their geometries. The structural variations arise from the combined effects of charge redistribution, depopulation of a ligand-based orbital, and population of a metal-based orbital (if it is not purely nonbonding).

The most significant structural distortion is found in the 3 LMCT state of **Fe-NNC**, in which the cyclometallating rings undergo substantial deviation from the mean plane of the N²N²C ligand, resulting in a huge relaxation and most probably very poor photophysical properties, unlike its Fe(II) analogue.¹⁸ Heavy mixing with GS'/GS", which appear unusually destabilized (0.62-0.75 eV instead of <0.5 eV), may be the reason for this abnormal behaviour. On average (excluding **Fe-NNC**) the energy gain between the Franck-Condon region and the relaxed 3 LMCT geometry amounts to 0.28 eV (ranging from 0.24 eV for **Fe-tpy**, to 0.31 eV for **Fe-tpy-NCN**), i.e. larger than the two reported Stokes shifts for emissive Fe(III) complexes,^{38,25} and larger than the 0.15 eV relaxation reported for the 3 MLCT states of their Fe(II) analogues.¹⁷ The average root mean square deviation between 3 GS and 3 LMCT geometries (excluding **Fe-NNC**) amounts to 0.092, and ranges between 0.053 (**Fe-tpy-NNC**) and 0.136 (**Fe-tpy-NCN**). Overall there is a slight contraction of the coordination sphere in the lowest 3 LMCT excited state, as seen in the average metal-ligand distance, accompanied by significant bond elongations within the ligand skeleton (e.g. from 1.398 to 1.427 Å, subsequent to the depopulation of C-C bonding orbitals in **Fe-tpy-NCN**, see Fig. S3). A contraction of the coordination sphere goes opposite to the reaction coordinate towards MC states, therefore a significant reorganization energy is expected to be involved in LMCT-to-MC conversions, which is interesting from the photophysical viewpoint.³⁶

The major excitation(s) describing the optimized 3 LMCT state of **Fe-tpy-NNC** is plotted in Figure 4, and in Figures S6-S10 for the other five complexes. The donating orbital is located on one tpy ligand in **Fe-tpy**, mostly on the phenyl ring (with some Fe contribution) in **Fe-tpy-NNC**

and **Fe-tpy-NCN**, and mostly on the phenyl ring(s) of the N[^]N[^]C ligand(s) in **Fe-NNC**, and **Fe-NNC-NCN**. On the other hand, **Fe-NCN**, is unique in the fact that its donating orbital is here mostly localized on the two Fe-C σ -bonds (Fig. S9). The receiving orbital is purely d_{π} in character for **Fe-tpy**, and has some contributions from bpy or tpy moieties in the cyclometallated complexes. The best photophysical capacities are expected in the absence of low-lying MC states that would tend to favor nonradiative quenching of the emission (quantification of the coupling between the lowest 3 LMCT state and these low-lying 3 MC states is out of the scope of this study).

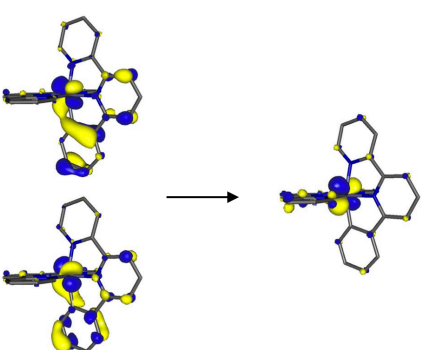
major excitations	adiabatic energy	vertical energy	S ²	f _{osc}
	2.03 eV	1.88 eV 661 nm	1.00	0.050230855

Figure 4: Characteristics of the optimized 3 LMCT state of **Fe-tpy-NNC**. At this geometry this state is the third state, following GS'/GS'' (0.33-0.47 eV). The adiabatic energy is the energy gap with the optimized 3 GS. The vertical energy corresponds to the potentially emitted photon.

Among the series, the most promising complex is therefore **Fe-tpy-NNC**, possessing a lowest 3 LMCT state with no potentially deactivating MC states below it, and a potential emission wavelength of 661 nm as computed in implicit acetonitrile. Note that this complex has been reported in the Fe(II) oxidation state, in which the cyclometallating ligand resulted in a still short but significantly increased 3 MLCT lifetime (0.8 ps vs 145 fs for Fe(tpy)₂²⁺).²¹ As shown by Bauer

et al., the first oxidation process is fully reversible, thus, provided the Fe(III) complex can be prepared on purpose, its photophysical characterization should be feasible.

The other five complexes of the series all bear ^1MC or MC-rich states below their optimized lowest $^3\text{LMCT}$ state, which should jeopardize their photophysical properties if the low-lying ^1MC states are indeed providing efficient nonradiative deactivation funnels (note that the reported emissive Fe(III) complex with ns $^3\text{LMCT}$ lifetime displays a low-lying ^1MC state)¹³. On the other hand, some could nevertheless prove interesting, this time for their MLCT states. Bauer's group indeed reported dual emission from $^3\text{LMCT}$ (675 nm) and $^3\text{MLCT}$ (450 nm) origin in a unique complex in which Fe(III) is bound by two car-cy-car ligands (car=carbene; cy=cyclometallating ligand).²⁵

MLCT state optimization

As presumed from the ground state TD-DFT data, $^3\text{LMCT}$ optimization has confirmed the presence of low-lying ^1MC states that should jeopardize the photophysical properties of **Fe-tpy**, **Fe-tpy-NCN** and **Fe-NCN**. Therefore MLCT excited state optimization was focused on the remaining two candidates, **Fe-NNC**, and **Fe-NNC-NCN**, for which LMCT-based emission is unlikely to be efficient for the aforementioned reasons.

For **Fe-NNC-NCN**, MLCT optimization converged but on a spin-contaminated state ($S^2 = 2.04$), shown in Figure S11. For **Fe-NNC**, the converged state was of quartet spin multiplicity ($S^2 = 2.66$). It is built on two major components, of MLCT and MC nature, slightly in favor of the MLCT character (Figure 5), and bears a moderate oscillator strength, in line with a formally spin-forbidden quartet-doublet transition. In agreement with the TD-DFT data at the ground state geometry, the optimized quartet state of MLCT+MC character was found at an

adiabatic energy of 1.80 eV and a vertical energy of 1.43 eV, corresponding to a potential emission at 869 nm. The MC character induces significant bond elongations (Table S10), which are associated with a massive 0.8 eV relaxation energy (this state appeared 2.19 eV above the ground state, at the ^3GS geometry).

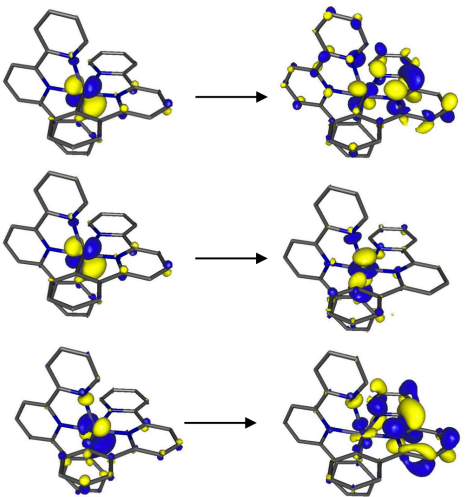
major excitations	adiabatic energy	vertical energy	S^2	f_{osc}
	1.80 eV	1.43 eV 869 nm	2.66	0.002481029

Figure 5: Characteristics of the optimized $\{^1\text{MLCT+MC}\}$ state of **Fe-NNC**. At this geometry this state is the third state, following GS'/GS'' (0.33-0.42 eV). The adiabatic energy is the energy gap with the optimized ^3GS . The vertical energy corresponds to the potentially emitted photon.

Conclusion

To conclude on the insight brought by excited state optimization, an emission is predicted from the formally third state (recall GS' and GS''), which is of $^3\text{LMCT}$ nature for **Fe-tpy-NNC** (661 nm) but of $\{^1\text{MLCT+MC}\}$ nature for **Fe-NNC**, (869 nm). This computational study has revealed important insights into the electronic structure and geometries of yet unreported $^3\text{LMCT}$

states of Fe(III) complexes. Whether they are specific to these particular cyclometallated complexes, or general to Fe(III) complexes, remains to be discovered by pursuing the experimental and computational effort towards other classes of Fe(III) luminophores. Improved systems would definitely require optimal oscillator strength, emission wavelength, and excited state lifetime to open up applications as fluorescent emitters or photoredox catalysts.

Supporting Information. The following files are available free of charge.

MO diagrams for the doublet ground states; TD-DFT at the doublet ground state geometries; geometrical parameters for the optimized GS, LMCT, and MLCT states; characteristics of the optimized LMCT and MLCT states (PDF)

Cartesian coordinates for optimized GS, LMCT, and MLCT states (zipped folder containing xyz files).

Acknowledgements : We thank the supercomputing facility of Toulouse University, CALMIP, for the allocation of resources (Project P18013). This manuscript is dedicated to Jean-Paul Collin and Jean-Louis Heully.

ABBREVIATIONS

DFT, density functional theory; TD-DFT, time-dependent DFT; LMCT, ligand-to-metal charge transfer; MLCT, metal-to-ligand charge transfer; MC, metal-centered.

REFERENCES

- (1) Wenger, O. S. Photoactive Complexes with Earth-Abundant Metals. *J. Am. Chem. Soc.* **2018**, *140* (42), 13522–13533. <https://doi.org/10.1021/jacs.8b08822>.
- (2) Förster, C.; Heinze, K. Photophysics and Photochemistry with Earth-Abundant Metals –

Fundamentals and Concepts. *Chem. Soc. Rev.* **2020**, *49* (4), 1057–1070. <https://doi.org/10.1039/C9CS00573K>.

(3) Behm, K.; McIntosh, R. D. Application of Discrete First-Row Transition-Metal Complexes as Photosensitisers. *ChemPlusChem* **2020**, *85* (12), 2611–2618. <https://doi.org/10.1002/cplu.202000610>.

(4) Wegeberg, C.; Wenger, O. S. Luminescent First-Row Transition Metal Complexes. *JACS Au* **2021**, *1* (11), 1860–1876. <https://doi.org/10.1021/jacsau.1c00353>.

(5) Gourdon, L.; Cariou, K.; Gasser, G. Phototherapeutic Anticancer Strategies with First-Row Transition Metal Complexes: A Critical Review. *Chem. Soc. Rev.* **2022**, *51* (3), 1167–1195. <https://doi.org/10.1039/D1CS00609F>.

(6) Larsen, C. B.; Wenger, O. S. Photoredox Catalysis with Metal Complexes Made from Earth-Abundant Elements. *Chem. - Eur. J.* **2018**, *24*, 2039–2058. <https://doi.org/10.1002/chem.201703602>.

(7) Dierks, P.; Vukadinovic, Y.; Bauer, M. Photoactive Iron Complexes: More Sustainable, but Still a Challenge. *Inorg. Chem. Front.* **2022**, *9*, 206–220. <https://doi.org/10.1039/D1QI01112J>.

(8) Monat, J. E.; McCusker, J. K. Femtosecond Excited-State Dynamics of an Iron(II) Polypyridyl Solar Cell Sensitizer Model. *J. Am. Chem. Soc.* **2000**, *122*, 4092–4097. <https://doi.org/10.1021/ja992436o>.

(9) Liu, Y.; Harlang, T.; Canton, S. E.; Chábera, P.; Suárez-Alcántara, K.; Fleckhaus, A.; Vithanage, D. A.; Göransson, E.; Corani, A.; Lomoth, R.; Sundström, V.; Wärnmark, K. Towards Longer-Lived Metal-to-Ligand Charge Transfer States of Iron(II) Complexes: An N-Heterocyclic Carbene Approach. *Chem. Commun.* **2013**, *49*, 6412–6414. <https://doi.org/10.1039/c3cc43833c>.

(10) Duchanois, T.; Etienne, T.; Cebrián, C.; Liu, L.; Monari, A.; Beley, M.; Assfeld, X.; Haacke, S.; Gros, P. C. An Iron-Based Photosensitizer with Extended Excited-State Lifetime: Photophysical and Photovoltaic Properties: An Iron-Based Photosensitizer with Extended Excited-State Lifetime. *Eur. J. Inorg. Chem.* **2015**, 2469–2477. <https://doi.org/10.1002/ejic.201500142>.

(11) Zimmer, P.; Burkhardt, L.; Friedrich, A.; Steube, J.; Neuba, A.; Schepper, R.; Müller, P.; Flörke, U.; Huber, M.; Lochbrunner, S.; Bauer, M. The Connection between NHC Ligand Count and Photophysical Properties in Fe(II) Photosensitizers: An Experimental Study. *Inorg. Chem.* **2018**, *57*, 360–373. <https://doi.org/10.1021/acs.inorgchem.7b02624>.

(12) Braun, J. D.; Lozada, I. B.; Kolodziej, C.; Burda, C.; Newman, K. M. E.; van Lierop, J.; Davis, R. L.; Herbert, D. E. Iron(II) Coordination Complexes with Panchromatic Absorption and Nanosecond Charge-Transfer Excited State Lifetimes. *Nat. Chem.* **2019**, *11*, 1144–1150. <https://doi.org/10.1038/s41557-019-0357-z>.

(13) Kjær, K. S.; Kaul, N.; Prakash, O.; Chábera, P.; Rosemann, N. W.; Honarfar, A.;

Gordivska, O.; Fredin, L. A.; Bergquist, K.-E.; Häggström, L.; Ericsson, T.; Lindh, L.; Yartsev, A.; Styring, S.; Huang, P.; Uhlig, J.; Bendix, J.; Strand, D.; Sundström, V.; Persson, P.; Lomoth, R.; Wärnmark, K. Luminescence and Reactivity of a Charge-Transfer Excited Iron Complex with Nanosecond Lifetime. *Science* **2019**, *363*, 249–253. <https://doi.org/10.1126/science.aau7160>.

(14) Prakash, O.; Lindh, L.; Kaul, N.; Rosemann, N. W.; Losada, I. B.; Johnson, C.; Chábera, P.; Ilic, A.; Schwarz, J.; Gupta, A. K.; Uhlig, J.; Ericsson, T.; Häggström, L.; Huang, P.; Bendix, J.; Strand, D.; Yartsev, A.; Lomoth, R.; Persson, P.; Wärnmark, K. Photophysical Integrity of the Iron(III) Scorpionate Framework in Iron(III)–NHC Complexes with Long-Lived ²LMCT Excited States. *Inorg. Chem.* **2022**, *61*, 17515–17526. <https://doi.org/10.1021/acs.inorgchem.2c02410>.

(15) Dixon, I. M.; Alary, F.; Boggio-Pasqua, M.; Heully, J.-L. The (N₄C₂)²⁻ Donor Set as Promising Motif for Bis(Tridentate) Iron(II) Photoactive Compounds. *Inorg. Chem.* **2013**, *52*, 13369–13374. <https://doi.org/10.1021/ic402453p>.

(16) Dixon, I. M.; Khan, S.; Alary, F.; Boggio-Pasqua, M.; Heully, J.-L. Probing the Photophysical Capability of Mono and Bis(Cyclometallated) Fe(II) Polypyridine Complexes Using Inexpensive Ground State DFT. *Dalton Trans.* **2014**, *43*, 15898–15905. <https://doi.org/10.1039/C4DT01939C>.

(17) Dixon, I. M.; Alary, F.; Boggio-Pasqua, M.; Heully, J.-L. Reversing the Relative ³MLCT–³MC Order in Fe(II) Complexes Using Cyclometallating Ligands: A Computational Study Aiming at Luminescent Fe(II) Complexes. *Dalton Trans.* **2015**, *44*, 13498–13503. <https://doi.org/10.1039/C5DT01214G>.

(18) Leis, W.; Argüello Cordero, M. A.; Lochbrunner, S.; Schubert, H.; Berkefeld, A. A Photoreactive Iron(II) Complex Luminophore. *J. Am. Chem. Soc.* **2022**, *144*, 1169–1173. <https://doi.org/10.1021/jacs.1c13083>.

(19) Mukherjee, S.; Bowman, D. N.; Jakubikova, E. Cyclometalated Fe(II) Complexes as Sensitizers in Dye-Sensitized Solar Cells. *Inorg. Chem.* **2015**, *54*, 560–569. <https://doi.org/10.1021/ic502438g>.

(20) Ashley, D. C.; Mukherjee, S.; Jakubikova, E. Designing Air-Stable Cyclometalated Fe(II) Complexes: Stabilization via Electrostatic Effects. *Dalton Trans.* **2019**, *48*, 374–378. <https://doi.org/10.1039/C8DT04402C>.

(21) Steube, J.; Burkhardt, L.; Pöpcke, A.; Moll, J.; Zimmer, P.; Schoch, R.; Wölper, C.; Heinze, K.; Lochbrunner, S.; Bauer, M. Excited-State Kinetics of an Air-Stable Cyclometalated Iron(II) Complex. *Chem. – Eur. J.* **2019**, *25*, 11826–11830. <https://doi.org/10.1002/chem.201902488>.

(22) Tang, Z.; Chang, X.-Y.; Wan, Q.; Wang, J.; Ma, C.; Law, K.-C.; Liu, Y.; Che, C.-M. Bis(Tridentate) Iron(II) Complexes with a Cyclometalating Unit: Photophysical Property Enhancement with Combinatorial Strong Ligand Field Effect. *Organometallics* **2020**, *39*, 2791–2802. <https://doi.org/10.1021/acs.organomet.0c00149>.

(23) Estrada-Montaño, A. S.; Gries, A.; Oviedo-Fortino, J. A.; Torres-Gutierrez, C.; Grain-

- Hayton, A.; Marcial-Hernández, R.; Shen, L.; Ryabov, A. D.; Gaiddon, C.; Le Lagadec, R. Dibromine Promoted Transmetalation of an Organomercurial by $\text{Fe}(\text{CO})_5$: Synthesis, Properties, and Cytotoxicity of Bis(2- C_6H_4 -2'-Py-KC,N)Dicarbonyliron(II). *Organometallics* **2020**, *39*, 1842–1854. <https://doi.org/10.1021/acs.organomet.0c00107>.
- (24) Estrada-Montaño, A. S.; Ryabov, A. D.; Gries, A.; Gaiddon, C.; Le Lagadec, R. Iron(III) Pincer Complexes as a Strategy for Anticancer Studies. *Eur. J. Inorg. Chem.* **2017**, *2017* (12), 1673–1678. <https://doi.org/10.1002/ejic.201601350>.
- (25) Bauer, M.; Steube, J.; Pöpcke, A.; Bokareva, O.; Reuter, T.; Demeshko, S.; Schoch, R.; Hohloch, S.; Meyer, F.; Heinze, K.; Kühn, O.; Lochbrunner, S. Janus-Type Dual Emission of a Cyclometalated Iron(III) Complex. *Res. Sq.* **2020**. <https://doi.org/10.21203/rs.3.rs-64316/v1>.
- (26) Law, K.-C.; Tang, Z.; Wu, L.; Wan, Q.; To, W.-P.; Chang, X.; Low, K.-H.; Liu, Y.; Che, C.-M. Cyclometalated Iron and Ruthenium Complexes Supported by a Tetradentate Ligand Scaffold with Mixed O, N, and C Donor Atoms: Synthesis, Structures, and Excited-State Properties. *Organometallics* **2022**, *41*, 418–429. <https://doi.org/10.1021/acs.organomet.1c00677>.
- (27) Reiher, M.; Salomon, O.; Artur Hess, B. Reparameterization of Hybrid Functionals Based on Energy Differences of States of Different Multiplicity. *Theor. Chem. Acc. Theory Comput. Model. Theor. Chim. Acta* **2001**, *107* (1), 48–55. <https://doi.org/10.1007/s00214-001-0300-3>.
- (28) Reiher, M. Theoretical Study of the $\text{Fe}(\text{Phen})_2(\text{NCS})_2$ Spin-Crossover Complex with Reparametrized Density Functionals. *Inorg. Chem.* **2002**, *41*, 6928–6935. <https://doi.org/10.1021/ic025891l>.
- (29) Grimme, S.; Antony, J.; Ehrlich, S.; Krieg, H. A Consistent and Accurate Ab Initio Parametrization of Density Functional Dispersion Correction (DFT-D) for the 94 Elements H-Pu. *J. Chem. Phys.* **2010**, *132*, 154104. <https://doi.org/10.1063/1.3382344>.
- (30) Grimme, S.; Ehrlich, S.; Goerigk, L. Effect of the Damping Function in Dispersion Corrected Density Functional Theory. *J. Comput. Chem.* **2011**, *32*, 1456–1465. <https://doi.org/10.1002/jcc.21759>.
- (31) van Wüllen, C. Molecular Density Functional Calculations in the Regular Relativistic Approximation: Method, Application to Coinage Metal Diatomics, Hydrides, Fluorides and Chlorides, and Comparison with First-Order Relativistic Calculations. *J. Chem. Phys.* **1998**, *109*, 392–399. <https://doi.org/10.1063/1.476576>.
- (32) Neese, F.; Wennmohs, F.; Becker, U.; Riplinger, C. The ORCA Quantum Chemistry Program Package. *J. Chem. Phys.* **2020**, *152* (22), 224108. <https://doi.org/10.1063/5.0004608>.
- (33) Weigend, F. Accurate Coulomb-Fitting Basis Sets for H to Rn. *Phys. Chem. Chem. Phys.* **2006**, *8*, 1057–1065. <https://doi.org/10.1039/b515623h>.
- (34) Allouche, A.-R. Gabedit-A Graphical User Interface for Computational Chemistry Softwares. *J. Comput. Chem.* **2011**, *32*, 174–182. <https://doi.org/10.1002/jcc.21600>.
- (35) Mukherjee, S.; Torres, D. E.; Jakubikova, E. HOMO Inversion as a Strategy for

Improving the Light-Absorption Properties of Fe(II) Chromophores. *Chem. Sci.* **2017**, *8*, 8115–8126. <https://doi.org/10.1039/C7SC02926H>.

(36) Larsen, C. B.; Braun, J. D.; Lozada, I. B.; Kunnus, K.; Biasin, E.; Kolodziej, C.; Burda, C.; Cordones, A. A.; Gaffney, K. J.; Herbert, D. E. Reduction of Electron Repulsion in Highly Covalent Fe-Amido Complexes Counteracts the Impact of a Weak Ligand Field on Excited-State Ordering. *J. Am. Chem. Soc.* **2021**, *143* (49), 20645–20656. <https://doi.org/10.1021/jacs.1c06429>.

(37) Brown, A. M.; McCusker, C. E.; McCusker, J. K. Spectroelectrochemical Identification of Charge-Transfer Excited States in Transition Metal-Based Polypyridyl Complexes. *Dalton Trans.* **2014**, *43*, 17635–17646. <https://doi.org/10.1039/C4DT02849J>.

(38) Chábera, P.; Liu, Y.; Prakash, O.; Thyraug, E.; Nahhas, A. E.; Honarfar, A.; Essén, S.; Fredin, L. A.; Harlang, T. C. B.; Kjær, K. S.; Handrup, K.; Ericson, F.; Tatsuno, H.; Morgan, K.; Schnadt, J.; Häggström, L.; Ericsson, T.; Sobkowiak, A.; Lidin, S.; Huang, P.; Styring, S.; Uhlig, J.; Bendix, J.; Lomoth, R.; Sundström, V.; Persson, P.; Wärnmark, K. A Low-Spin Fe(III) Complex with 100-Ps Ligand-to-Metal Charge Transfer Photoluminescence. *Nature* **2017**, *543*, 695–699. <https://doi.org/10.1038/nature21430>.